A Quasi open-loop robust three-phase grid-synchronization technique for non-ideal grid

Ahmed, Hafiz; Biricik, Samet; Benbouzid, Mohamed

IET Generation, Transmission & Distribution

DOI:
https://doi.org/10.1049/gtd2.12203

Published: 01/12/2021

Publisher's PDF, also known as Version of record

Received: 10 December 2020 | Revised: 10 February 2021 | Accepted: 22 April 2021

IET Generation, Transmission & Distribution

DOI: 10.1049/gtd2.12203

The Institution of Engineering and Technology WILEY

ORIGINAL RESEARCH PAPER

A Quasi open-loop robust three-phase grid-synchronization technique for non-ideal grid

Hafiz Ahmed[1] | **Samet Biricik**[2,3] | **Mohamed Benbouzid**[4,5]

[1] Nuclear Futures Institute, Bangor University, Bangor LL57 1UT, United Kingdom

[2] Department of Electrical and Electronics Engineering, European University of Lefke, Lefke, Northern Cyprus, TR-10 Mersin, Turkey

[3] School of Electrical and Electronic Engineering, Technological University Dublin, Dublin, Ireland

[4] University of Brest, UMR CNRS 6027 IRDL, France

[5] Logistics Engineering College, Shanghai Maritime University, Shanghai, China

Correspondence
Hafiz Ahmed, Nuclear Futures Institute, Bangor University, Bangor LL57 1UT, UK.
Email: hafiz.h.ahme@ieee.org

Abstract

Development of advanced grid-synchronization technique for unbalanced and distorted grid is considered in this paper. In this context, self-tuning filter (STF) is considered to extract the fundamental component from the measured unbalanced and distorted voltages. Standard STF considers balanced grid voltages which is not always possible to ensure in the actual power grid. To mitigate this issue, an extended STF is proposed by analyzing the standard STF in the state-space framework. To make the proposed ESTF grid-following, a robust open-loop frequency estimator is also applied. The closed-loop system enjoys excellent filtering benefit from the extended STF side while taking advantage of the fast convergence speed property of the open-loop frequency estimation technique. Numerical simulation and experimental results with double second-order generalized integrator phase-locked loop are provided to validate the theoretical developments.

1 | INTRODUCTION

Grid-interfacing converters (GIC) [1–13] are almost ubiquitous in today's modern power system. GICs are used to integrate distributed energy sources, generate DC voltage through active rectification of the grid voltage, improve the power quality through active power filtering, maintain constant voltage at the sensitive load, emulate the grid voltage for power converter testing etc. All these applications highlight the importance of GIC. In-phase operation of GICs with the grid is often required to ensure efficient control of GICs.

In-phase operation requires an accurate estimate of the grid parameters which is often obtained through grid-synchronization techniques. Zero-crossing detection (ZCD) [14, 15] is undoubtedly one of the simplest approach in this regard. By detecting the zero-crossing, phase and frequency of any periodic sinusoidal signal can easily be obtained. However, if the signal is not ideal and sinusoidal and the measured signal is corrupted with noise, then erroneous detection may happen which will degrade the performance. ZCD exploits the sinusoidal and periodic nature of the grid voltage signal. Discrete Fourier transform (DFT) [16] also exploits the same property. If it is assumed that the grid frequency is constant, then theoretically speaking, DFT is a highly efficient technique for grid parameters estimation. In practice, this assumption is often violated. To mitigate this issue, large window length is needed for the digital implementation of DFT. High memory requirements come with higher computational demand as well. This could limit the digital implementation of DFT in low computational power-based embedded devices. Using basic trigonometric expansion formula, the grid voltage can be efficiently written in the parametric form. This enables the application of regression-type parameter estimation algorithms [17, 18]. To preserve the linear nature of the parametric model, an addition frequency estimator is often used in regression-type techniques. This together with weights tuning often make the design process of this type of techniques complicated.

Phase-locked loop (PLL) [19–26] provides an estimation of the grid voltage parameters by using a combination of phase detector and a low-pass filter. Traditional PLL often referred as the synchronous reference frame PLL (SRF-PLL) assumes that the grid voltages have same magnitude, that is, voltages are balanced. To mitigate this problem, additional filters are often used to generate balance set of voltages. Some popular filters

that are often used with PLL are second-order generalized integrator (SOGI) [15, 27–30], adaptive notch filter (ANF) [31], double decoupled synchronous reference frame (DDSRF) [20], self-tuning filter (STF) [32, 33], moving average filter (MAF) [34], delayed signal cancellation [35] etc. Tuning the control gains of PLL under the presence of additional filtering stage is not straightforward. PLL is closed-loop technique where the stability is not unconditional. The control parameters greatly affect the stability of PLL.

In recent times, several modifications of SRF-PLL are proposed in the literature. Out of them, double synchronous reference frame PLL (DSRF-PLL) [36] is undoubtedly one of the most popular one. However, this technique is computationally complex as four low-pass filters and complex trigonometric calculations are required to extract the fundamental frequency positive sequence components. Multiple complex coefficient filter (MCCF) PLL [37] also require several filters which increases the computational complexity. Similarly, cascaded DSC PLL as proposed in [38] also requires a large number of filters.

Open-loop or pseudo open-loop [39–42] techniques recently garnered some attention in the literature. This type of techniques estimate the grid frequency without using feedback. This can help to achieve fast convergence. However, pre-filtering is often required to reduce the effect of noise and distortion in the estimated frequency. Such a pre-filter based open-loop technique is recently reported by Safa et al. in [39] using self-tuning filter (STF) [43]. This approach combines the best of both world. From the filtering aspect, this technique benefits from the excellent band-pass filtering property of the STF while can provide fast convergence thanks to the open-loop frequency estimation approach.

STF has already gained its place in the literature as an excellent band-pass filter having fast dynamic response characteristics. Wide applications of STF are already reported in the literature [32, 33]. Despite the attractive features of STF as presented in [39, 44], this technique is not suitable for unbalanced voltages. Balanced voltage assumption is often not realistic in the actual power grid. As such there are scopes to further enhance the performance of the STF in unbalanced and distorted grid scenario.

The focus of this paper is on enhancing the performance of STF for unbalanced and distorted grid application. For this purpose, an extended STF (ESTF) is proposed. The development of the proposed ESTF is based on first analyzing the STF in state-space. By extending the state-space model of STF with respect to Park-transformed unbalanced voltages, the proposed ESTF is obtained. In addition, a robust open-loop frequency estimator is applied to make sure that the ESTF can follow the grid. These modifications make the proposed ESTF robust to unbalance and distortions.

Organization of this paper is as follows: Brief overview and analysis of the STF are given in Section 2. Details of the proposed extension of the STF are provided in Section 3. Development of the robust open-loop frequency estimation technique is detailed in Section 4. Results and discussions are available in Section 5, and finally, Section 6 provides some concluding remarks.

2 | SELF-TUNING FILTER: AN OVERVIEW

2.1 | Voltage signal transformation

Unbalanced three-phase grid voltages are typically modelled as

$$\Xi_r = \underbrace{\Xi^+ \sin\left(\omega t + \varphi^+\right)}_{\Xi_r^+} + \underbrace{\Xi^- \sin\left(\omega t + \varphi^-\right)}_{\Xi_r^-}, \tag{1a}$$

$$\Xi_g = \underbrace{\Xi^+ \sin\left(\omega t - \frac{2\pi}{3} + \varphi^+\right)}_{\Xi_g^+} + \underbrace{\Xi^- \sin\left(\omega t + \frac{2\pi}{3} + \varphi^-\right)}_{\Xi_g^-}, \tag{1b}$$

$$\Xi_b = \underbrace{\Xi^+ \sin\left(\omega t + \frac{2\pi}{3} + \varphi^+\right)}_{\Xi_b^+} + \underbrace{\Xi^- \sin\left(\omega t - \frac{2\pi}{3} + \varphi^-\right)}_{\Xi_b^-}, \tag{1c}$$

where the individual phases are denoted by r, g, b, positive and negative sequence components are denoted by the superscript $+$ and $-$, respectively. In Equation (1), the grid frequency is denoted by ω, the initial phase angle is denoted by φ and the amplitude is denoted by Ξ. When the voltages are balanced, in that case $\Xi^- = 0$. In this case, the reduced-order Clarke transformation ($\alpha\beta-$frame) [45] can be applied to reduce the three-phase voltages into two quadrature voltages as given below:

$$\Xi^b_{\alpha\beta} = \underbrace{\sqrt{\frac{2}{3}}\begin{bmatrix} \sqrt{\frac{2}{3}} & -\sqrt{\frac{1}{6}} & -\sqrt{\frac{1}{6}} \\ 0 & -\sqrt{\frac{1}{2}} & \sqrt{\frac{1}{2}} \end{bmatrix}}_{\mathcal{T}_{\alpha\beta}} \Xi^b_{rgb}, \tag{2}$$

where $\Xi^b_{\alpha\beta} = [\Xi^b_\alpha \quad \Xi^b_\beta]^T$ and $\Xi^b_{rgb} = [\Xi^+_r \quad \Xi^+_g \quad \Xi^+_b]^T$ with the superscript b indicating that the voltages are being balanced. By simplifying the Equation (2), the quadrature voltages are found as:

$$\Xi^b_\alpha = \Xi^+ \sin(\omega t + \varphi^+), \tag{3a}$$

$$\Xi^b_\beta = \Xi^+ \cos(\omega t + \varphi^-). \tag{3b}$$

Standard self-tuning filter is based on the Clark-transformed grid voltages (3). In this work, it is assumed that the grid voltages could be unbalanced, that is, Ξ^- is not always equal to zero. In this case, transformation (2) with unbalanced grid voltages could be written as:

$$\Xi_{\alpha\beta} = \mathcal{T}_{\alpha\beta}\Xi_{rgb}, \tag{4}$$

where $\Xi_{\alpha\beta} = [\Xi_\alpha \quad \Xi_\beta]^T$ and $\Xi_{rgb} = [\Xi_r \quad \Xi_g \quad \Xi_b]^T$. Equation (4) can be simplified as:

$$\Xi_\alpha = \underbrace{\Xi^+ \sin\left(\omega t + \varphi^+\right)}_{\Xi_\alpha^+} + \underbrace{\Xi^- \sin\left(\omega t + \varphi^-\right)}_{\Xi_\alpha^-}, \tag{5a}$$

$$\Xi_\beta = \underbrace{\Xi^+ \cos\left(\omega t + \varphi^+\right)}_{\Xi_\beta^+} - \underbrace{\Xi^- \cos\left(\omega t + \varphi^-\right)}_{\Xi_\beta^-}. \tag{5b}$$

Equations (5a) and (5b) are combination of positive and negative sequence components. Using the positive and negative sequence components in $\alpha\beta$, the sequences in the original frame, that is, *rgb* can be obtained as:

$$\begin{bmatrix} \Xi_r^+ \\ \Xi_g^+ \\ \Xi_b^+ \end{bmatrix} = \sqrt{\frac{3}{2}} \begin{bmatrix} \sqrt{\frac{2}{3}} & 0 \\ -\sqrt{\frac{1}{6}} & \sqrt{\frac{1}{2}} \\ -\sqrt{\frac{1}{6}} & -\sqrt{\frac{1}{2}} \end{bmatrix} \begin{bmatrix} \Xi_\alpha^+ \\ \Xi_\beta^+ \end{bmatrix}, \tag{6a}$$

$$\begin{bmatrix} \Xi_r^- \\ \Xi_g^- \\ \Xi_b^- \end{bmatrix} = \sqrt{\frac{3}{2}} \begin{bmatrix} \sqrt{\frac{2}{3}} & 0 \\ -\sqrt{\frac{1}{6}} & \sqrt{\frac{1}{2}} \\ -\sqrt{\frac{1}{6}} & -\sqrt{\frac{1}{2}} \end{bmatrix} \begin{bmatrix} \Xi_\alpha^- \\ \Xi_\beta^- \end{bmatrix}. \tag{6b}$$

2.2 | Overview of the self-tuning filter

Time and frequency domain equations of the self-tuning filter are given by [32, 39, 43]:

$$\hat{\Xi}^b_{\alpha\beta}(t) = \mathrm{e}^{j\omega t} \int_0^\tau \mathrm{e}^{-j\omega\tau} \Xi^b_{\alpha\beta}(\tau) d\tau, \tag{7a}$$

$$\frac{\hat{\Xi}^b_{\alpha\beta}}{\Xi^b_{\alpha\beta}}(s) = \mathrm{STF}(s) = \frac{s + j\omega}{s^2 + \omega^2}. \tag{7b}$$

where output of the filter is denoted by the $\hat{}$. The dynamic response of filter (7) is not user tunable. This can be made user tunable by introducing a positive gain η in the transfer function (6b) as given below:

$$G(s) = \frac{s + \eta + j\omega}{(s + \eta)^2 + \omega^2}. \tag{8}$$

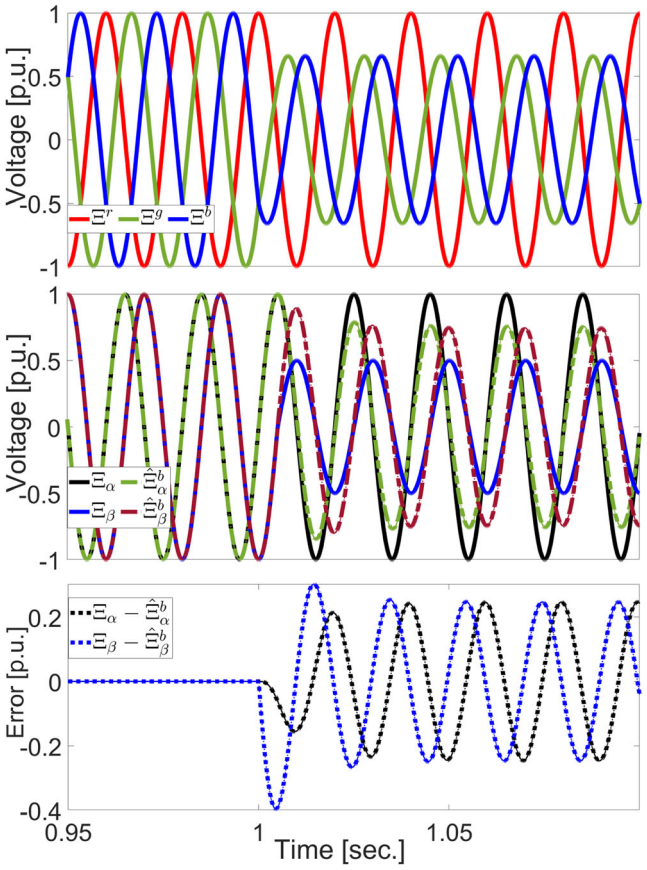

FIGURE 1 Numerical simulation results with $\eta = 100$

Filter (7) in state-space observer framework could be written as:

$$\dot{\hat{\Xi}}^b_{\alpha\beta} = A\hat{\Xi}^b_{\alpha\beta} + L\left(y - C\hat{\Xi}^b_{\alpha\beta}\right), \tag{9a}$$

$$y = C\hat{\Xi}^b_{\alpha\beta}, \tag{9b}$$

where $y = \hat{\Xi}^b_{\alpha\beta}$ is the output and

$$A = \begin{bmatrix} 0 & -\omega \\ \omega & 0 \end{bmatrix}, L = \begin{bmatrix} \eta & 0 \\ 0 & \eta \end{bmatrix}, C = \begin{bmatrix} 1 & 0 \\ 0 & 1 \end{bmatrix}.$$

Eigenvalues of the closed-loop error system are: $-\eta \pm i\omega$. Since the tuning parameter η is positive by design choice, the filter (7) is always stable. In designing the self-tuning filter, it is assumed that all the phases have same amplitude. In practice, this can not be always guaranteed. As such, unbalanced amplitudes among phases will have serious impact on the performance of self-tuning filter. To test the performance of the conventional self-tuning filter (7), let us consider unbalance fault in the grid as shown in Figure 1. Results show that the self-tuning filter is sensitive to unbalance fault as the estimation errors are significantly high. To obtain the results of Figure 1, $\eta = 100$ is used. It is to be noted here that as the STF does not

consider the grid to be unbalanced, steady-state estimation error is inevitable for any positive values of η as long as the grid remain unbalanced. To mitigate the issue of unbalanced grid, extended self-tuning filter is proposed in this paper. The proposed extended version can handle the effects of negative and zero sequence components. Details are discussed in the next section.

3 | PROPOSED EXTENDED SELF-TUNING FILTER

Our focus in this section is to extend the self-tuning filter (9) for the unbalanced grid in the $\alpha\beta$ coordinate (5). To facilitate this, let us assume that the states are $\xi_1 = \Xi_\alpha^+$, $\xi_2 = \Xi_\beta^+$, $\xi_3 = \Xi_\alpha^-$, $\xi_4 = \Xi_\beta^-$, and $\xi = [\xi_1\ \xi_2\ \xi_3\ \xi_4]^T$. With respect to the state vector ξ, the unbalanced grid can be modelled as:

$$\dot{\xi} = \mathcal{A}\xi, \tag{10a}$$

$$y = C\xi, \tag{10b}$$

where $y = [\Xi_\alpha \quad \Xi_\beta]^T$ and

$$\mathcal{A} = \begin{bmatrix} 0 & -\omega & 0 & 0 \\ \omega & 0 & 0 & 0 \\ 0 & 0 & 0 & -\omega \\ 0 & 0 & \omega & 0 \end{bmatrix}, \quad C = \begin{bmatrix} 1 & 0 & 1 & 0 \\ 0 & 1 & 0 & -1 \end{bmatrix}.$$

For the system (10), the proposed ESTF in the state-space is given by:

$$\dot{\hat{\xi}} = \mathcal{A}\hat{\xi} + L(y - C\hat{\xi}), \tag{11a}$$

$$\hat{y} = C\hat{\xi}, \tag{11b}$$

where

$$L = \begin{bmatrix} \eta & 0 & \eta & 0 \\ 0 & \eta & 0 & -\eta \end{bmatrix}.$$

In (11), it is assumed that the grid frequency ω is known. However, this is not the case for actual power grid. This problem will be considered in the next section. Closed-loop poles of the observer error dynamics are: $-\eta \pm \sqrt{\eta^2 - \omega^2}$. Real part of the poles are always negative for any positive η and positive grid frequency ω. This makes the proposed filter stable. In addition, if the tuning gain η is chosen as $\eta < \omega$, then the closed-loop poles are always complex conjugate similar to the standard self-tuning filter. From (11), the following transfer functions

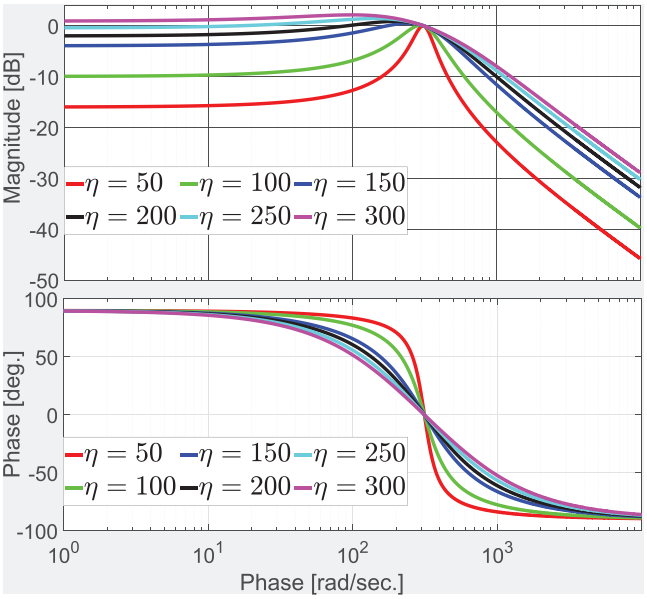

FIGURE 2 Frequency response of the proposed extended self-tuning filter

could be obtained:

$$\hat{\Xi}_\alpha^+(s) = \frac{\eta s \Xi_\alpha - \eta\omega\Xi_\beta}{s^2 + 2\eta s + \omega^2}, \tag{12a}$$

$$\hat{\Xi}_\alpha^-(s) = \frac{\eta s \Xi_\alpha + \eta\omega\Xi_\beta}{s^2 + 2\eta s + \omega^2}, \tag{12b}$$

$$\hat{\Xi}_\beta^+(s) = \frac{\eta\omega\Xi_\alpha + \eta s\Xi_\beta}{s^2 + 2\eta s + \omega^2}, \tag{12c}$$

$$\hat{\Xi}_\beta^-(s) = \frac{\eta\omega\Xi_\alpha - \eta s\Xi_\beta}{s^2 + 2\eta s + \omega^2}. \tag{12d}$$

Based on (12), the transfer functions for positive sequence components are given by:

$$\frac{\hat{\Xi}_\alpha^+(s) + j\hat{\Xi}_\beta^+(s)}{\Xi_\alpha(s) + j\Xi_\beta(s)} = \frac{\eta(s + j\omega)}{s^2 + 2\eta s + \omega^2}. \tag{13}$$

Based on the frequency response (Figure 2), it can be found that the proposed extended self-tuning filter has the band-pass characteristics as the existing self-tuning filter. Band-pass filtering property can be inferred from the magnitude plot in Figure 2. Magnitude plot shows that the ESTF allows only signals of particular frequency band to pass. For decreasing tuning gain η, one can see that the transfer function (13) becomes more and more frequency selective, that is, the width of the pass band becomes smaller. This property is very important as it will help ESTF to extract the fundamental component from the distorted grid voltages. The time constant of the proposed

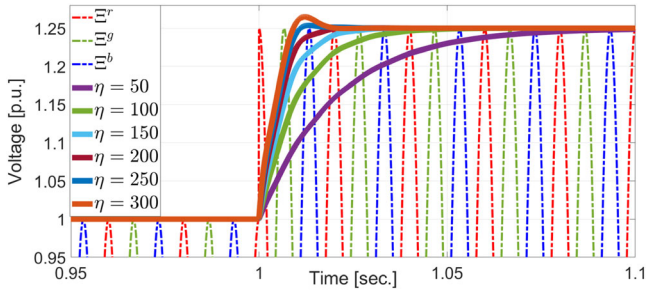

FIGURE 3 Time response of the ESTF when the grid voltage experience +0.25p.u.step change in the amplitude

filter depends on the tuning gain η. To demonstrate this, let us consider the time-response of the ESTF as shown in Figure 3. This figure shows that low value of η makes the dynamic response slower. So, frequency selectivity comes with high time constant. As such, tuning of η should be considered as a trade-off between frequency selectivity versus time constant. Block diagram of the proposed ESTF is given in Figure 4. Block diagram of the conventional STF is also given in this figure for comparison purpose.

To tune the proposed ESTF, transfer functions (13) can be considered. By comparing the denominator of this transfer function with the standard second-order transfer function $s^2 + 2\zeta\omega_o s + \omega_0^2$, one can find that $\eta = \zeta\omega_o$. It is well known from the literature that $\zeta = 1/\sqrt{2}$ can be considered as an optimal factor. Then, by selecting cutoff frequency ω_o, the ESTF can easily be tuned.

3.1 | Dynamic performance of the ESTF

Time-domain solutions of transfer functions (12a) and (12c) are given by:

$$\hat{\Xi}_\alpha^+(t) = \Xi^+ \sin(\omega t + \varphi^+) - \Xi^+ e^{-\eta t} \sin(\varphi^+) \Big\{ \cosh(\mathcal{X} t) - \frac{\sinh(\mathcal{X} t)\{\eta \Xi^- \cos(\varphi^-) + \omega \Xi^+ \cos(\varphi^+)\}}{\mathcal{X} \Xi^+ \sin(\varphi^+)} \Big\}, \tag{14a}$$

$$\hat{\Xi}_\beta^+(t) = \Xi^+ \cos(\omega t + \varphi^+) - \Xi^+ e^{-\eta t} \cos(\varphi^+) \Big\{ \cosh(\mathcal{X} t) + \frac{\sinh(\mathcal{X} t)(\eta \Xi^- \sin(\phi^-) + \omega \Xi^+ \sin(\phi^+))}{\mathcal{X} \Xi^+ \cos(\phi^+)} \Big\}, \tag{14b}$$

where $\mathcal{X} = \sqrt{\mu^2 - \omega^2}$. Equations (14a) and (14b) have two parts. The second part in these equations are decaying exponential with a decay rate of η^{-1}. This decay rate controls the convergence speed of the proposed extended self-tuning filter.

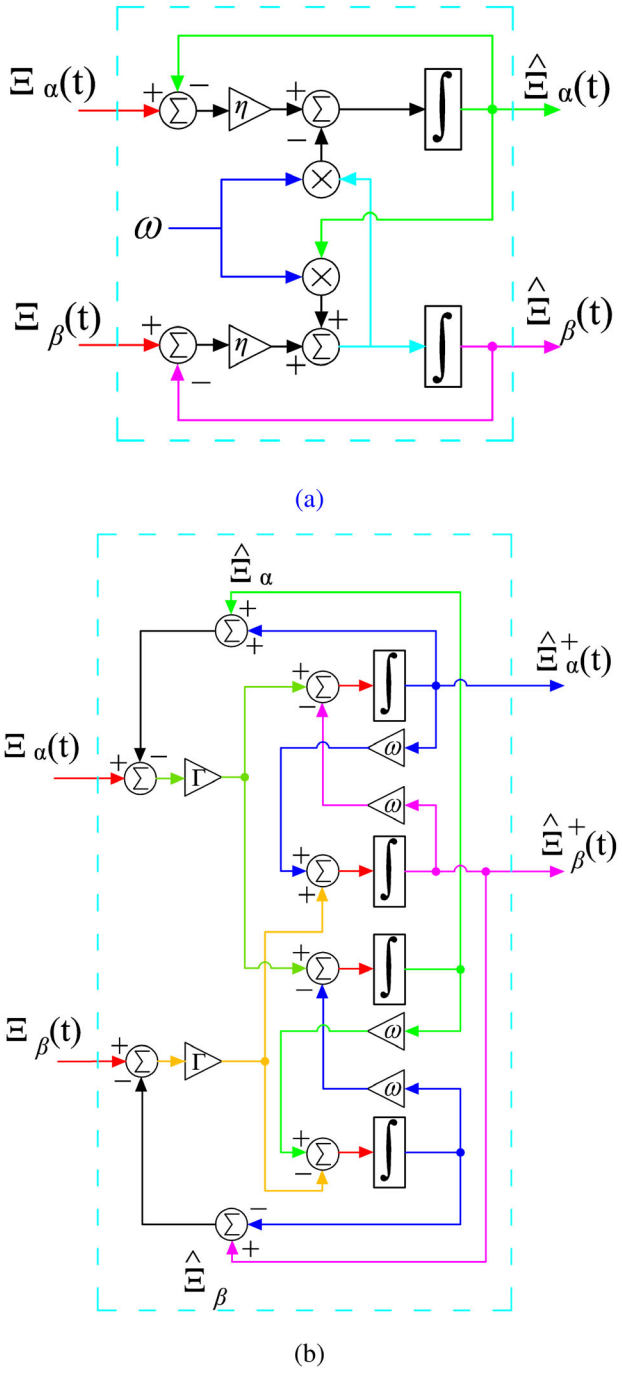

FIGURE 4 Block diagram of (a) conventional STF and (b) proposed ESTF

4 | FREQUENCY ESTIMATION

In developing the proposed extended self-tuning filter (Section 3), it was assumed that the grid frequency ω is known or an estimate is available. In practice, the actual frequency of the power grid is not a constant value. It continuously varies

within a specified limit, typically between 47 and 52 Hz according to EN50160 standard. So, accurate estimation of grid frequency is essential for the proper operation of the proposed filter. Out of various choices available in the literature in this regard, open-loop technique [39, 40, 46] has gained significant attraction is recent time. Unlike closed-loop techniques like PLL and FLL, open-loop technique has unconditional stability. This makes open-loop technique very attractive. Open-loop techniques often rely on the numerical estimation of the derivative of measured signals as shown below:

$$\tan^{-1}\left(\frac{\hat{\Xi}_{\alpha}^{+}}{\hat{\Xi}_{\beta}^{+}}\right)=\tan^{-1}\left\{\frac{\sin\left(\hat{\omega}t+\hat{\varphi}^{+}\right)}{\cos\left(\hat{\omega}t+\hat{\varphi}^{+}\right)}\right\},$$

$$\tan^{-1}\left(\frac{\hat{\Xi}_{\alpha}^{+}}{\hat{\Xi}_{b}^{+}}\right)=\hat{\omega}t+\hat{\varphi}^{+}. \tag{15}$$

By taking time derivative of Equation (15), the frequency can be obtained as:

$$\frac{d}{dt}\left(\hat{\omega}t+\hat{\varphi}^{+}\right)=\frac{d}{dt}\left\{\tan^{-1}\left(\frac{\hat{\Xi}_{\alpha}^{+}}{\hat{\Xi}_{b}^{+}}\right)\right\},$$

$$\hat{\omega}=\frac{\hat{\Xi}_{\beta}^{+}\dot{\hat{\Xi}}_{\alpha}^{+}-\hat{\Xi}_{\alpha}^{+}\dot{\hat{\Xi}}_{\beta}^{+}}{\left(\hat{\Xi}_{\alpha}^{+}\right)^{2}+\left(\hat{\Xi}_{\beta}^{+}\right)^{2}}. \tag{16}$$

As shown in Equation (16), the grid frequency can be obtained through calculating the derivative of the filtered signals $\hat{\Xi}_{\alpha}^{+}(t)$ and $\hat{\Xi}_{\beta}^{+}(t)$. Discrete-time implementation of the continuous-time derivative can be sensitive to sampling interval. To illustrate this, backward-Euler discretization is considered and the time is discretized as $t=k\Delta\mathcal{T}, k=0,1,2,\ldots,\infty$, where sampling interval and sampling instants are denoted by $\Delta\mathcal{T}$ and k, respectively. Then, the derivative of the filtered signals are given by [41]:

$$\begin{aligned}\dot{\hat{\Xi}}_{\alpha}^{+}(k)&=\Delta\mathcal{T}^{-1}\left\{\hat{\Xi}_{\alpha}^{+}(k)-\hat{\Xi}_{\alpha}^{+}(k-1)\right\},\\&=\Delta\mathcal{T}^{-1}\hat{\Xi}^{+}\sin(\omega k\Delta\mathcal{T}+\varphi)\\&\quad-\Delta\mathcal{T}^{-1}\hat{\Xi}^{+}\sin\left\{\omega(k-1)\Delta\mathcal{T}+\varphi\right\},\\&=\hat{\Xi}^{+}\Delta\mathcal{T}^{-1}\sin(\omega k\Delta\mathcal{T}+\varphi)\{1-\cos(\omega\Delta\mathcal{T})\}\\&\quad+\hat{\Xi}^{+}\Delta\mathcal{T}^{-1}\cos(\omega k\Delta\mathcal{T}+\varphi)\sin(\omega\Delta\mathcal{T}).\end{aligned} \tag{17}$$

$$\begin{aligned}\dot{\hat{\Xi}}_{\beta}^{+}(k)&=\Delta\mathcal{T}^{-1}\left\{\hat{\Xi}_{\beta}^{+}(k)-\hat{\Xi}_{\beta}^{+}(k-1)\right\},\\&=\Delta\mathcal{T}^{-1}\hat{\Xi}^{+}\cos(\omega k\Delta\mathcal{T}+\varphi)\\&\quad-\Delta\mathcal{T}^{-1}\hat{\Xi}^{+}\cos\left\{\omega(k-1)\Delta\mathcal{T}+\varphi\right\},\\&=\hat{\Xi}^{+}\Delta\mathcal{T}^{-1}\cos(\omega k\Delta\mathcal{T}+\varphi)\{1-\cos(\omega\Delta\mathcal{T})\}\\&\quad-\hat{\Xi}^{+}\Delta\mathcal{T}^{-1}\sin(\omega k\Delta\mathcal{T}+\varphi)\sin(\omega\Delta\mathcal{T}).\end{aligned} \tag{18}$$

By using the estimated derivatives (17) and (18) in Equation (16),:

$$\frac{\hat{\Xi}_{\beta}^{+}\dot{\hat{\Xi}}_{\alpha}^{+}-\hat{\Xi}_{\alpha}^{+}\dot{\hat{\Xi}}_{\beta}^{+}}{\left(\hat{\Xi}_{\alpha}^{+}\right)^{2}+\left(\hat{\Xi}_{\beta}^{+}\right)^{2}}=\frac{\sin(\omega\Delta\mathcal{T})}{\Delta\mathcal{T}},$$

$$\hat{\omega}=\Delta\mathcal{T}^{-1}\left\{\sum_{n=0}^{\infty}\frac{(-1)^{n}}{(2n+1)!}(\omega\Delta\mathcal{T})^{2n+1}\right\},$$

$$\hat{\omega}=\Delta\mathcal{T}^{-1}\left\{\omega\Delta\mathcal{T}-\frac{(\omega\Delta\mathcal{T})^{3}}{3!}+\cdots\right\},$$

$$\hat{\omega}\approx\omega-\frac{\omega^{3}(\Delta\mathcal{T})^{2}}{3!}. \tag{19}$$

In obtaining Equation (19), Taylor series expansion of the sine term is used. Moreover, higher order terms are ignored. For sufficiently small sampling interval, that is, $\Delta\mathcal{T}<<1$, the second term in Equation (19) can be ignored and one can find that $\hat{\omega}\approx\omega$. However, if the sampling interval is relatively large, in that case, the second term in Equation (19) can not be ignored and it needs to be compensated to mitigate the sampling related estimation error. To find the compensation term, let us assume that $\omega=\omega_0+\tilde{\omega}$, where the nominal frequency and the deviation are denoted by ω_0 and $\tilde{\omega}$. Then, Equation (19) can be written as:

$$\hat{\omega}\approx\omega_0+\tilde{\omega}-\frac{(\Delta\mathcal{T})^{2}}{3!}\left(\omega_0^{3}+3\omega_0^{2}\tilde{\omega}+3\omega_0\tilde{\omega}^{2}+\tilde{\omega}^{3}\right). \tag{20}$$

By ignoring the terms $3\omega_0\tilde{\omega}^2+\tilde{\omega}^3$ in Equation (20), it can be further simplified to

$$\hat{\omega}\approx\omega_0+\tilde{\omega}-\frac{(\Delta\mathcal{T})^{2}}{3!}\left(\omega_0^{3}+3\omega_0^{2}\tilde{\omega}\right),$$

$$\tilde{\omega}\approx\frac{\hat{\omega}-\omega_0+\frac{(\Delta\mathcal{T})^{2}}{3!}\omega_0^{3}}{1-\frac{(\Delta\mathcal{T})^{2}}{2!}\omega_0^{2}}. \tag{21}$$

The term $\tilde{\omega}$ provides an estimate of the frequency deviation which in turn can be used to estimate the unknown grid frequency. In obtaining Equation (21), higher-order terms are ignored. These terms can be prominent in very low sampling frequency or large frequency deviation case. To overcome this issue, a moving average filter (MAF) can be added with $T_w=T/2$, where T is the grid signal's period. Thanks to this MAF, complete error elimination is possible even at low sampling frequency operation. Overview of the frequency estimation technique is given in Figure 5.

An overview of the computations involved in the proposed technique and two other popular techniques available in the literature are given in Table 1.

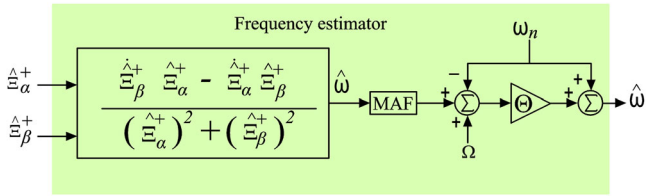

FIGURE 5 Frequency estimation technique used in this work

TABLE 1 An overview of the computations involved in the proposed technique, DSOGI-PLL [47], and DSRF-PLL [36]

	DSOGI	DSRF	Proposed
Phase Detector			
No. of integrators	4	0	1
No. of tuning gains	1	1	1
No. of MAF or LPF	0	4	0
Park transformation	Needed	Needed	No need
Frequency Estimator			
No. of tuning gains	2	2	1
No. of MAF or LPF	1	1	1
Harmonic robustness	Medium	Medium	High

5 | RESULTS AND DISCUSSIONS

This section reports the comparative analysis through numerical simulation and experimental validation. As a comparison tool, double second-order generalized integrator phase-locked loop (SOGI-PLL) [47] is selected. SOGI-PLL are selected as: SOGI gain, $k = \sqrt{2}$ and PLL gains, $k_p = 177.7$ and $k_i = 15971$. ESTF parameter is chosen as, $\Gamma = 150$. By considering a sampling frequency of 10 kHz,ESTF and SOGI-PLL are implemented in Matlab/Simulink.

5.1 | Simulation results

5.1.1 | Voltage sag test

A voltage sag of -0.3 p.u. is considered in this test. The simulation results are shown in Figure 6.

The frequency estimated by SOGI-PLL and ESTF converged in slightly more than 2 cycles. The peak frequency overshoot was more than 2 Hz for the SOGI-PLL while it was $\approx$ 1.5 Hz for the proposed ESTF. Same performance can be seen for amplitude and phase estimation error as well. From the phase estimation error results, it can be seen that the proposed ESTF has a faster rise time compared to SOGI-PLL.

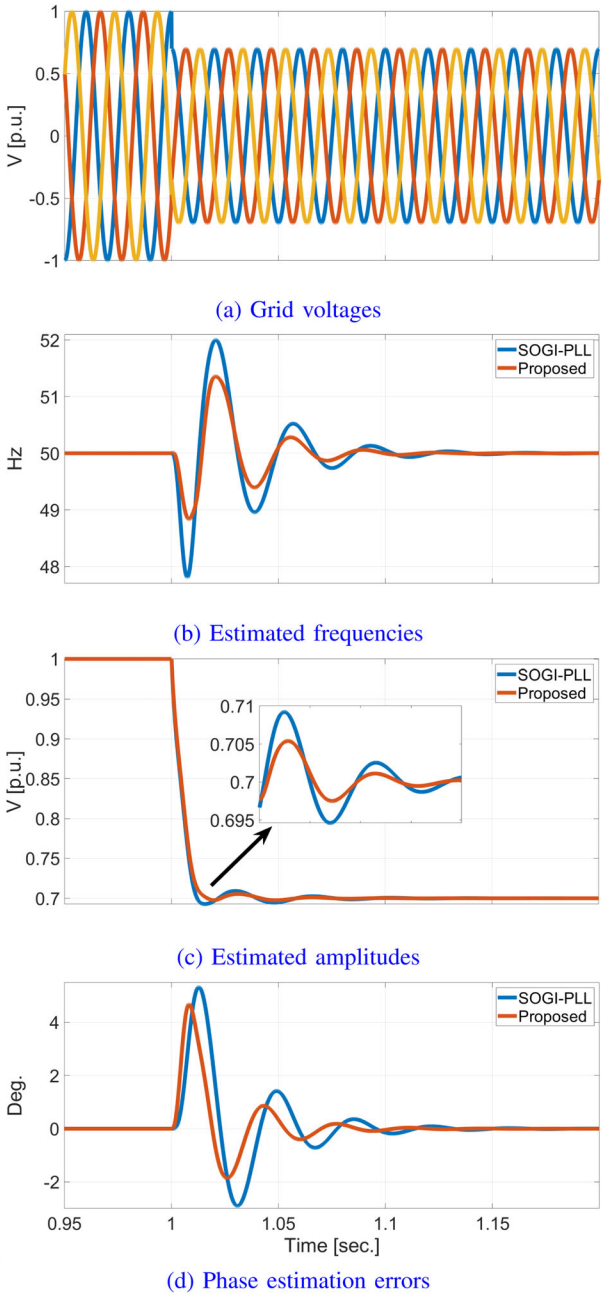

FIGURE 6 Simulation results for -0.3 p.u. voltage sag in the balanced grid

5.1.2 | Unbalance test

Initially, balanced grid is considered, that is, $\Xi^+ = 1\angle 0°$ and $\Xi^- = 0$. Suddenly, the grid became $\Xi^+ = 0.7\angle 0°$ and $\Xi^- = 0.3\angle 0°$. Simulation results are shown in Figure 7. The peak frequency and amplitude estimation overshoots are $\approx$ 50% smaller for the proposed technique. Comparatively faster convergence for the phase estimation error can be observed for the proposed ESTF as well. These results show that the proposed ESTF is very suitable for unbalanced grid.

5.1.3 | Distorted grid test

A distorted grid is considered in this test. The distortions comprised $5.8\% - 5^{\text{th}}$, $4.4\% - 7^{\text{th}}$ order, $4.5\% - 11^{\text{th}}$ order,

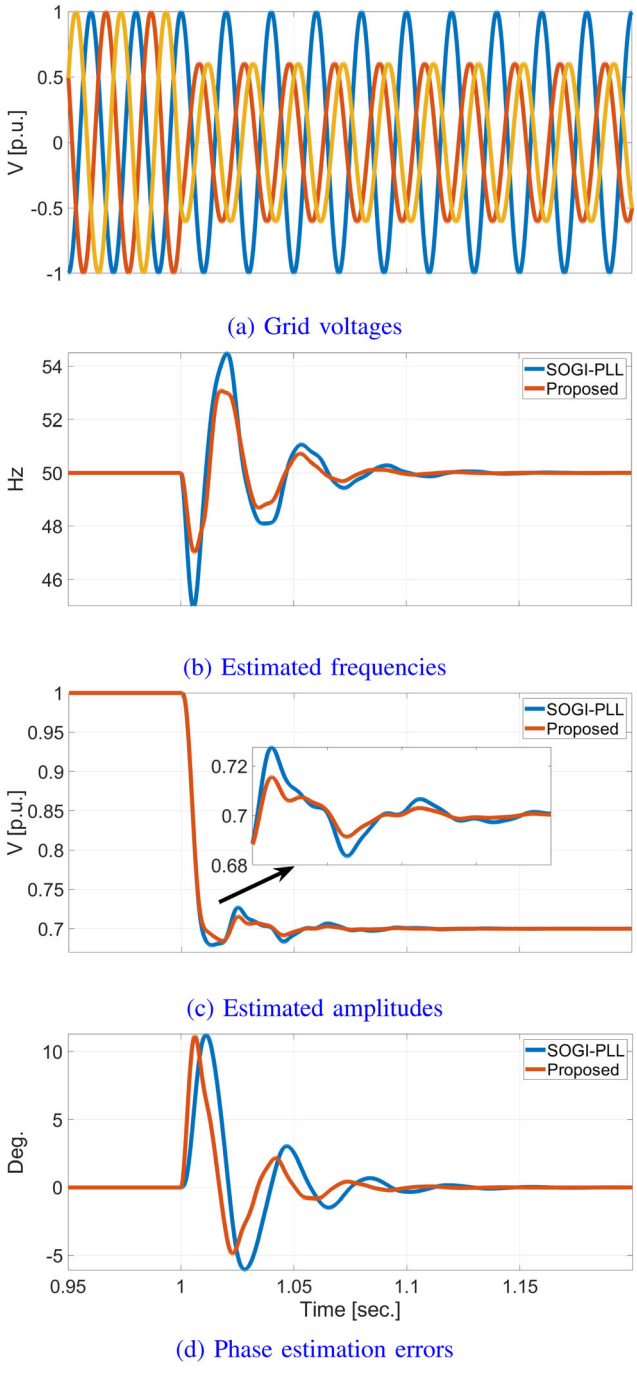

FIGURE 7 Simulation results for unbalanced fault in the grid

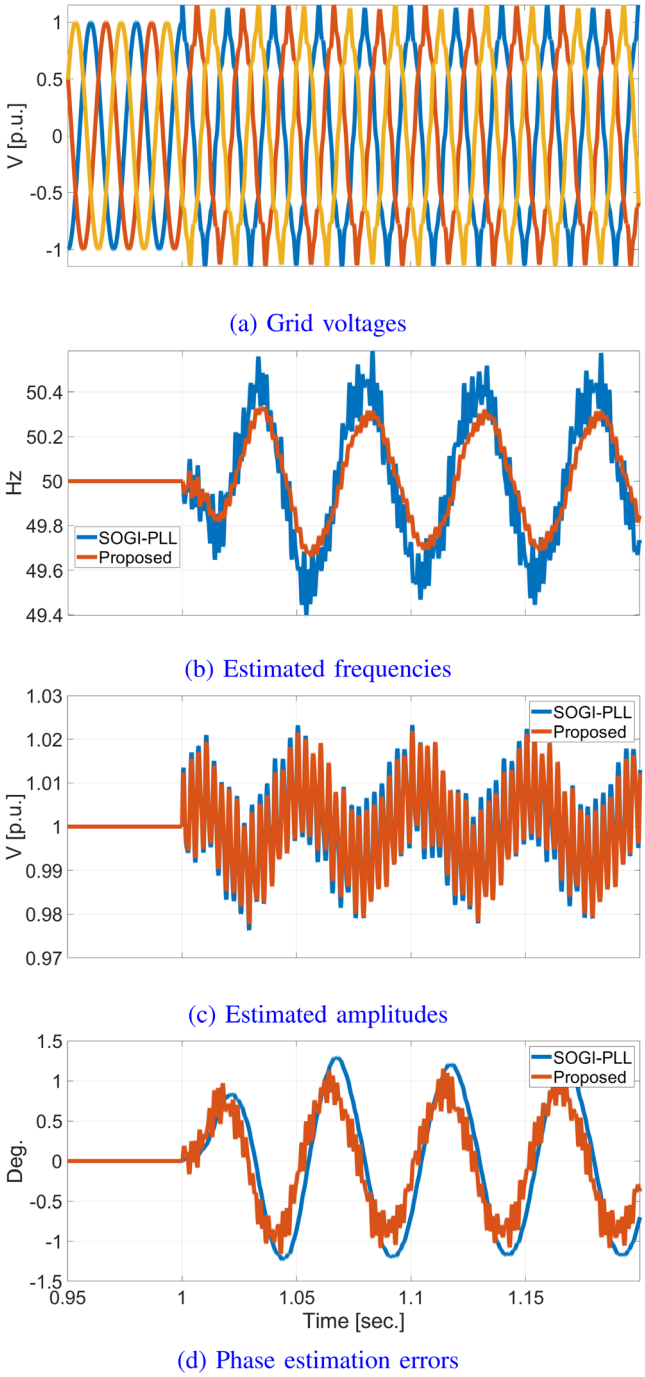

FIGURE 8 Simulation results for distorted grid voltage signals

1.1% − 30 Hz sub-harmonics, and 1.7% − 420 Hz inter-harmonics. The grid has a overall total harmonic distortion (THD) of 9.45%. Simulation results are given in Figure 8. The presence of inter and sub-harmonics make it very challenging for the comparative techniques. The frequency and phase estimation error ripples are smaller for the proposed technique compared to SOGI-PLL. SOG-PLL has a proportional-integral loop filter which is a low-pass filter. The proposed technique estimates the phase directly from the filtered signals at the output of the ESTF without any additional filtering. Despite this, the proposed technique showed better performance compared to SOGI-PLL. The THD of the signal filtered by the SOGI-PLL is 1.03% where as it is 0.9% for the ESTF. This is another advantage of the proposed technique if sequence component extraction aspect is considered. Grid-connection standards [48, 49] specify that the THD should be less than 5%. In this regard, the proposed technique also complies with the standards.

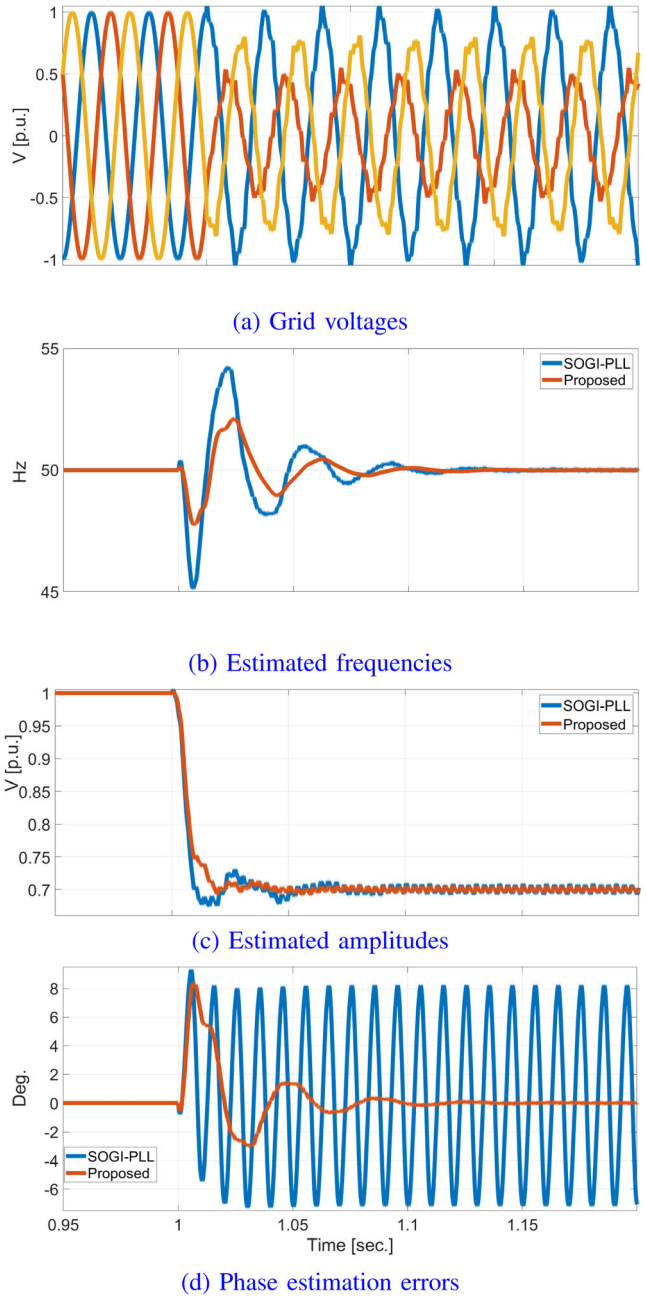

FIGURE 9 Simulation results for unbalanced and distorted grid voltage signals

5.1.4 | Unbalance and distorted grid test

In this test, unbalance and distortions are considered at the same time. The distortions comprise $2.8\% - 5^{th}$, $2.4\% - 7^{th}$ order, $2.9\% - 11^{th}$ order, $1.7\% - 13^{th}$ order, and $1.1\% - 19^{th}$ order harmonics. The unbalance grid parameters are $\Xi^{+} = 0.7\angle 0°$ and $\Xi^{-} = 0.3\angle 0°$. Numerical simulation results are given in Figure 9. The phase estimation errors as shown in Figure 9(d) demonstrate that the proposed technique can eliminate the steady-state ripple induced by the presence of odd-harmonics thanks to the moving average filter. Both SOGI-PLL and the proposed technique have similar convergence time.

TABLE 2 Comparative time domain performance summary

	SOGI-PLL	Proposed
Voltage sag test		
Settling time (±0.1 Hz)	97 ms	68 ms
Settling time (±0.1°)	98 ms	72 ms
Frequency overshoot	2.2 Hz	1.35 Hz
Phase overshoot	5.33°	4.68°
Unbalance est		
Settling time (±0.1 Hz)	105 ms	77 ms
Settling time (±0.1°)	124 ms	97 ms
Frequency overshoot	5.05 Hz	2.98 Hz
Phase overshoot	11.2°	11.1°
Distorted grid test		
Settling time (±0.1 Hz)	NA	NA
Settling time (±0.1°)	NA	NA
Frequency overshoot	0.58 Hz	0.32 Hz
Phase overshoot	1.3°	1.1°
Distorted & unbalanced grid test		
Settling time (±0.1 Hz)	112 ms	88 ms
Settling time (±0.1°)	NA	92.6 ms
Frequency overshoot	4.9 Hz	1.9 Hz
Phase overshoot	9.3°	8.3°

*NA, Not Applicable as the steady-state value was outside of the band.

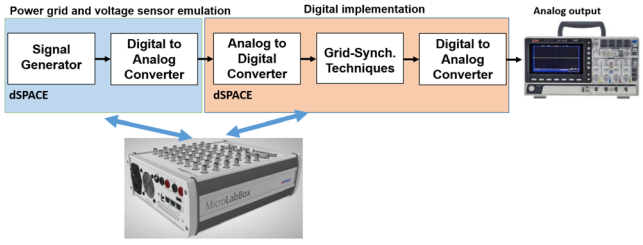

FIGURE 10 Overview of the considered hardware-in-the-loop setup

A comparative summary of the simulation tests are presented in Table 2.

5.2 | Experimental validation

Experimental results are reported in this section using dSPACE-based platform. To generate the grid voltages, a hardware-in-the-loop setup is used similar to [39]. Overview of the considered setup is given in Figure 10. The following tests are considered for experimental validation:

- Experimental Test-I: Frequency step change of −2 Hz
- Experimental Test-II: Amplitude step change of −0.5 p.u.
- Experimental Test-III: Diode rectifier induced harmonics

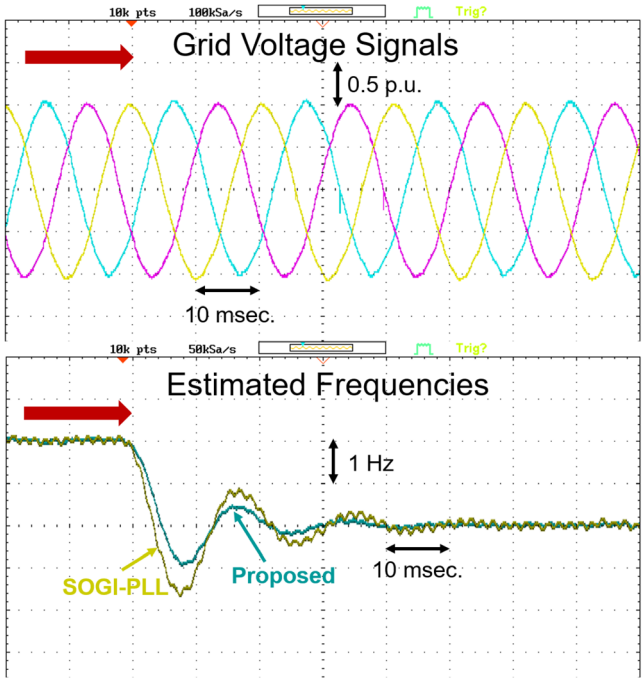

FIGURE 11 Comparative results for Experimental Test-I

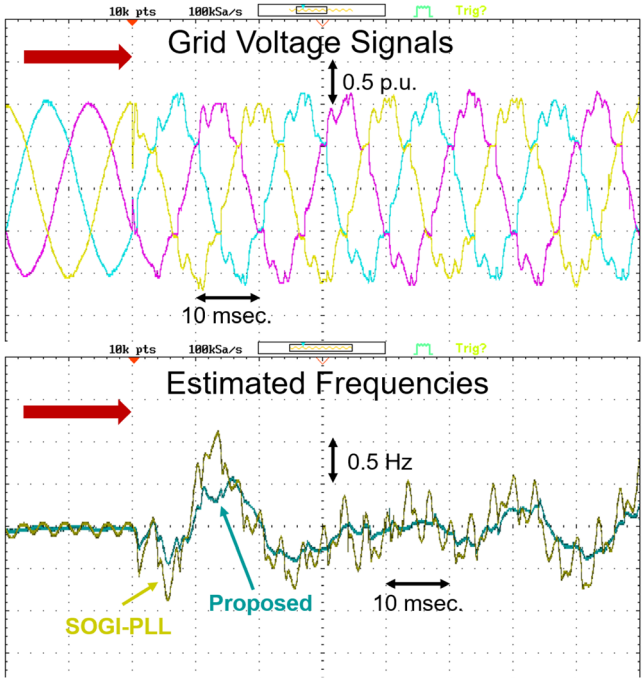

FIGURE 13 Comparative results for Experimental Test-III

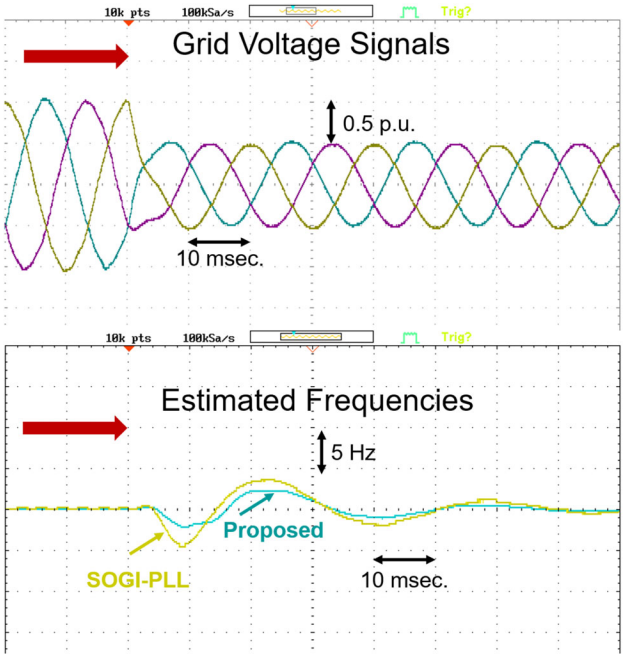

FIGURE 12 Comparative results for Experimental Test-II

Experimental results for Test-I are shown in Figure 11. Both techniques converged within 2 cycles. SOGI-PLL showed a 50% higher peak overshoot than the proposed method. This can play an important role in maintaining the stability of the grid-connected converter when the grid undergoes a sudden large in system frequency.

Experimental results for Test-II are given in Figure 12. Sudden large voltage sag had a serious impact in the frequency estimation. Both techniques took more than two cycles to converge. Similar to Test-I, the proposed technique had significantly smaller frequency overshoot compared to the SOGI-PLL. This justifies the suitability of the proposed approach to handle large voltage sag. According to many grid-codes [50], grid-connected converters need to be connected even in the presence of the large voltage sag. Exceptional performance by the proposed technique show that this approach is very suitable to provide low-voltage ride through (LVRT) capability to grid-connected converters.

The considered converter output voltages have a total harmonic distortion (THD) of approximately 2%. When the diode rectifier is connected, the THD became more than 12%. This case is considered in Test-III and the results are shown in Figure 13. Results in Figure 13 show that both techniques generate estimation ripple when the grid became heavily distorted. The proposed technique uses moving average filter whereas SOGI-PLL uses low-pass filter. Results in Figure 13 show that the frequency estimated by the proposed technique is much smoother than the SOGI-PLL and also has a lower estimation ripple. This demonstrate that the extended self-tuning filter as proposed in this paper is very suitable even in a heavily distorted grid.

6 | CONCLUSION AND FUTURE WORKS

An extended self-tuning filter is proposed in this paper to achieve grid-following operation of grid-interactive inverters. The grid-following operation is ensured by an open-loop frequency estimator which is robust to harmonic disturbances. The proposed extension is inspired by the standard self-tuning filter which is originally designed for balanced grid. Both

standard self-tuning filter and the proposed extension have similar frequency domain characteristics. Comparative results demonstrated that the proposed extended self-tuning filter can accurately and quickly extract the fundamental component of the positive sequence voltages from non-ideal grid voltages.

In this work, MAF has been used in the frequency estimator. Subject to the window length selection, MAF can slow down the convergence speed. To overcome this issue, phase-lead compensator can be used. By applying Padé approximation, MAF can be approximated as a first-order or second-order filter. Then the delay induced by this filter can be eliminated by designing an appropriate phase-lead compensator. Such an approach has recently been considered in [34]. Applying similar approach to the proposed technique will be considered as a future work. Similarly, pre-loop filter approach as proposed in [42] can also be considered to provide additional harmonic robustness. This work selects the window length of MAF as half of the nominal period. This does not provide DC-offset rejection. To add DC-offset rejection, low-pass filter-based approach as proposed in [28] will also be considered as a future work. Moreover, small-signal model of the proposed technique will also be considered in a future work. Application of the proposed grid-synchronization technique to various interesting applications such as active power filter and dynamic voltage restorer will be considered in a future work.

ORCID

Hafiz Ahmed https://orcid.org/0000-0001-8952-4190
Mohamed Benbouzid https://orcid.org/0000-0002-4844-508X

REFERENCES

1. Said-Romdhane, M.B., Skander-Mustapha, S., Slama-Belkhodja, I.: Robust dynamic grid emulator control. Comput. Electr. Eng. 85, 106663 (2020)
2. Safa, A., et al.: A robust control algorithm for a multifunctional grid tied inverter to enhance the power quality of a microgrid under unbalanced conditions. Int. J. Electr. Power Energy Syst. 100, 253–264 (2018)
3. Saxena, H., Singh, A., Rai, J.N.: Adaptive spline-based PLL for synchronisation and power quality improvement in distribution system. IET Gener. Transm. Distrib. 14(7), 1311–1319 (2020)
4. Bayhan, S., Abu-Rub, H.: A simple control technique for distributed generations in grid-connected and islanded modes. In: 2018 IEEE 27th International Symposium on Industrial Electronics (ISIE), pp. 1237–1242. IEEE, Piscataway, NJ (2018)
5. Trabelsi, M., et al.: Finite-control-set model predictive control for grid-connected packed-U-cells multilevel inverter. IEEE Trans. Ind. Electron. 63(11), 7286–7295 (2016)
6. Kumar, A., et al.: CC-ROGI-FLL based control for grid-tied photovoltaic system at abnormal grid conditions. IET Gener. Transm. Distrib. 14(17), 3400–3411 (2020)
7. Biricik, S., et al.: Super twisting sliding mode control of DVR with frequency-adaptive Brockett oscillator. IEEE Transaction on Industrial Electronics. (2020)
8. Zhou, Z., et al.: Tidal stream turbine control: an active disturbance rejection control approach. Ocean Eng. 202, 107190 (2020)
9. Pandey, S.K., Singh, B., Modi, G.: Frequency-adaptive complex-coefficient filter-based control for grid-integrated PV system. IET Gener. Transm. Distrib. 14(19), 4141–4151 (2020)
10. Pal, K., et al.: Sigmoidal and Gaussian functions based neural neuron technique for grid interactive solar energy system enabling power quality improvement. IET Gener. Transm. Distrib. 14(23), 5471–5479 (2020)
11. Verma, A.K., et al.: Improved fundamental frequency estimator for three-phase application. IEEE Trans. Ind. Electron. (2020)
12. Bayhan, S., Komurcugil, H.: Sliding-mode control strategy for three-phase three-level T-type rectifiers with DC capacitor voltage balancing. IEEE Access 8, 64555–64564 (2020)
13. Ahmed, H., Benbouzid, M.: On the enhancement of generalized integrator-based adaptive filter dynamic tuning range. IEEE Trans. Instrum. Meas. 69(10), 7449–7457 (2020)
14. Wall, R.: Simple methods for detecting zero crossing. In: IECON'03. 29th Annual Conference of the IEEE Industrial Electronics Society (IEEE Cat. No. 03CH37468), vol. 3, pp. 2477–2481. IEEE, Piscataway, NJ (2003)
15. Busarello, T.D.C., Junior, S.L.S., da Silva, N.: Zero-crossing detection frequency estimator method combined with a Kalman filter for non-ideal power grid. In: 2019 IEEE 15th Brazilian Power Electronics Conference and 5th IEEE Southern Power Electronics Conference (COBEP/SPEC), pp. 1–6. IEEE, Piscataway, NJ (2019)
16. McGrath, B.P., Holmes, D.G., Galloway, J.J.H.: Power converter line synchronization using a discrete Fourier transform (DFT) based on a variable sample rate. IEEE Trans. Power Electron. 20(4), 877–884 (2005)
17. Terriche, Y., Guerrero, J.M., Vasquez, J.C.: Performance improvement of shunt active power filter based on non-linear least-square approach. Electr. Power Syst. Res. 160, 44–55 (2018)
18. Amirat, Y., et al.: Phasor estimation for grid power monitoring: least square vs. linear Kalman filter. Energies 13(10), 2456 (2020)
19. Ullah, I., Ashraf, M.: Comparison of synchronization techniques under distorted grid conditions. IEEE Access 7, 101345–101354 (2019)
20. Sevilmiş, F., Karaca, H.: Performance analysis of SRF-PLL and DDSRF-PLL algorithms for grid interactive inverters. Int. Adv. Res. Eng. J. 3(2), 116–122 (2019)
21. Bechouche, A., et al.: An adaptive neural PLL for grid synchronization. In: IECON 2012-38th Annual Conference on IEEE Industrial Electronics Society, pp. 4451–4456. IEEE, Piscataway, NJ (2012)
22. Chedjara, Z., et al.: A novel robust PLL algorithm applied to the control of a shunt active power filter using a self tuning filter concept. In: 2018 IEEE International Conference on Industrial Technology (ICIT), pp. 1124–1131. IEEE, Piscataway, NJ (2018)
23. Kaura, V., Blasko, V.: Operation of a phase locked loop system under distorted utility conditions. IEEE Trans. Ind. Appl. 33(1), 58–63 (1997)
24. Quraan, M.: Error compensation algorithm for SRF-PLL in three-phase grid-connected converters. IEEE Access 8, 182338–182346 (2020)
25. Kamil, H.S., et al.: Recent advances in phase-locked loop based synchronization methods for inverter-based renewable energy sources. Indones. J. Electrical Eng. Comput. Sci. 18(1), 1–8 (2020)
26. Eltarouty, A., et al.: Unbalance and Disturbance Rejection Based Phase Locked Loop for Grid Synchronization. In: IECON 2020 The 46th Annual Conference of the IEEE Industrial Electronics Society, pp. 4967–4972. IEEE, Piscataway, NJ (2020)
27. Rodriguez, P., et al.: Advanced grid synchronization system for power converters under unbalanced and distorted operating conditions. In: IEEE Industrial Electronics, IECON 2006-32nd Annual Conference on IEEE Industrial Electronics, pp. 5173–5178. IEEE, Piscataway, NJ (2006)
28. Kherbachi, A., et al.: Enhanced structure of second-order generalized integrator frequency-locked loop suitable for DC-offset rejection in single-phase systems. Electr. Power Syst. Res. 170, 348–357 (2019)
29. Bendib, A., et al.: SOGI-FLL based optimal current control scheme for single-phase grid-connected photovoltaic VSIs with LCL Filter. In: 2018 International Conference on Electrical Sciences and Technologies in Maghreb (CISTEM), pp. 1–6. IEEE, Piscataway, NJ (2018)
30. Bendib, A., et al.: New modeling approach of secondary control layer for autonomous single-phase microgrids. J. Franklin Inst. 356(13), 6842–6874 (2019)
31. Mekhilef, S., Tarek, M., Abd Rahim, N.: Single-phase hybrid active power filter with adaptive notch filter for harmonic current estimation. IETE J. Res. 57(1), 20–28 (2011)
32. Biricik, S., et al.: Real-time control of shunt active power filter under distorted grid voltage and unbalanced load condition using self-tuning filter. IET Power Electron. 7(7), 1895–1905 (2014)

33. Ngo, T., Biricik, S., Basu, M.: A self-tuning grid synchronization method for active power filters. Electr. Power Compon. Syst. 44(17), 1947–1957 (2016)
34. Liu, C., et al.: Enhanced grid-connected phase-locked loop based on a moving average filter. IEEE Access 8, 5308–5315 (2019)
35. Rasheduzzaman, M., Kimball, J.W.: Modeling and tuning of an improved delayed-signal-cancellation PLL for microgrid application. IEEE Trans. Energy Convers. 34(2), 712–721 (2018)
36. Rodríguez, P., et al.: Decoupled double synchronous reference frame PLL for power converters control. IEEE Trans. Power Electron. 22(2), 584–592 (2007)
37. Terriche, Y., et al.: Multiple-complex coefficient-filter-based PLL for improving the performance of shunt active power filter under adverse grid conditions. In: 2018 IEEE Power & Energy Society General Meeting (PESGM), pp. 1–5. IEEE, Piscataway, NJ (2018)
38. Hamed, H.A., et al.: Frequency adaptive CDSC-PLL using axis drift control under adverse grid condition. IEEE Trans. Ind. Electron. 64(4), 2671–2682 (2017)
39. Safa, A., et al.: A Pseudo open loop synchronization technique for heavily distorted grid voltage. Electr. Power Syst. Res. 158, 136–146 (2018)
40. Terriche, Y., et al.: Adaptive CDSC-based open-loop synchronization technique for dynamic response enhancement of active power filters. IEEE Access 7, 96743–96752 (2019)
41. Golestan, S., et al.: A true open-loop synchronization technique. IEEE Trans. Ind. Inf. 12(3), 1093–1103 (2016)
42. Verma, A.K., et al.: An improved hybrid prefiltered open-loop algorithm for three-phase grid synchronization. IEEE Trans. Ind. Electron. 68(3), 2480–2490 (2021)
43. Abdusalam, M., et al.: New digital reference current generation for shunt active power filter under distorted voltage conditions. Electr. Power Syst. Res. 79(5), 759–765 (2009)
44. Ahmed, H., Biricik, S., Benbouzid, M.: Extended self-tuning filter-based synchronization technique for unbalanced and distorted grid. In: 2020 2nd International Conference on Smart Power Internet Energy Systems (SPIES), pp. 350–355 (2020)
45. Duesterhoeft, W., Schulz, M.W., Clarke, E.: Determination of instantaneous currents and voltages by means of alpha, beta, and zero components. Trans. Am. Inst. Electr. Eng. 70(2), 1248–1255 (1951)
46. Ahmed, H., et al.: Adaptive filtering-based Pseudo open-loop three-phase grid-synchronization technique. Energies 13(11), 2927 (2020)
47. Ranjan, A., Kewat, S., Singh, B.: DSOGI-PLL with in-loop filter based solar grid interfaced system for alleviating power quality problems. IEEE Trans. Ind. Appl. (2020)
48. Commission IE, et al.: Characteristics of the utility interface for photovoltaic (PV) systems. Report of IEC 61727, (2002)
49. Basso, T.S., DeBlasio, R.: IEEE 1547 series of standards: interconnection issues. IEEE Trans. Power Electron. 19(5), 1159–1162 (2004)
50. Wu, Y.K., Lin, J.H., Lin, H.J.: Standards and guidelines for grid-connected photovoltaic generation systems: A review and comparison. IEEE Trans. Ind. Appl. 53(4), 3205–3216 (2017)

How to cite this article: Ahmed, H., Biricik, S., Benbouzid, M.: A Quasi open-loop robust three-phase grid-synchronization technique for non-ideal grid. *IET Gener. Transm. Distrib.* 1–12 (2021). https://doi.org/10.1049/gtd2.12203